Journal of Alloys and Compounds 781 (2019) 186–195

Contents lists available at ScienceDirect

Journal of Alloys and Compounds

journal homepage: http://www.elsevier.com/locate/jalcom

Enhanced mechanical and tribological properties of V-Al-C coatings via increasing columnar boundaries

Zhenyu Wang, Hao Kang, Rende Chen, Peiling Ke**, Aiying Wang*

Key Laboratory of Marine Materials and Related Technologies, Zhejiang Key Laboratory of Marine Materials and Protective Technologies, Ningbo Institute of Materials Technology and Engineering, Chinese Academy of Sciences, Ningbo 315201, China

ARTICLE INFO

Article history:
Received 16 August 2018
Received in revised form
13 November 2018
Accepted 16 November 2018
Available online 3 December 2018

Keywords:
V-Al-C
Nanostructure
Amorphous carbon
Columnar boundaries
Toughness

ABSTRACT

Grain size, growth morphology, and grain boundary were considered to affect hardness and fracture toughness of hard coatings. An effective approach is currently developed to improve their hardness and toughness via tailoring their architectures through grain boundary control. V-Al-C coatings consisting of variable architectures were prepared by reactive sputtering V_2AlC target with different CH_4 flow rates in this study. The results indicated that, when the carbon content increased from 37.32 at.% to 71.4 at.%, the microstructure of V-Al-C coatings was tailored to span a wide changes from coarse columnar grain to fibrous columnar grains and finally to nanocomposite structure consisted of the (V, Al)C nanocrystallites and sp^2-rich a-C. Especially, the maximum hardness of 28.74 GPa and the excellent toughness with high H/E value of 0.11 were obtained once the coating displayed fibrous columnar structure, such good mechanical properties benefited the lowest wear rate of 2.8×10^{-16} m^3/Nm. Instead, the nanocomposite structure showed the lower fracture resistance due to the dominated amorphous carbon matrix. All coatings with nanocomposite structure exhibited low friction coefficient of ~0.18, which was attributed to the coupling lubrication originated from both V_2O_5 Magnéli phases and amorphous carbon formed during friction process. The enhanced mechanical and tribological properties were also discussed in terms of the columnar boundaries evolution as a function of carbon content.

1. Introduction

During the last years, binary transition metal nitrides (TMN) or carbides (TMC) hard coatings have been extensively used to enhance the wear-resistance properties of mechanical components, i.e., cutting, forming and machining tools [1–4]. To maximize the operation efficiency of mechanical components, various ternary and quaternary hard coatings by multicomponent alloying have been fabricated to obtain the combination of superior mechanical properties, good fracture toughness as well as high oxidation resistance [5], such as Ti-Al-N [6], Ti-Al-Si-N [7], Cr-Si-N [8], Cr-B-N [9], Ti-Al-B-N [10] and Ti-Cr-Al-N [11]. Nevertheless, these coatings suffer from relatively high friction coefficient during the dry machining processes, which are extremely serious for Ti- or Cr-based hard coatings. Recently, it is found that the V-based coating presents a low friction and wear in a wide temperature range (293–993 K) [12,13], due to the formation of V_2O_5 self-lubricant phase, called Magnéli phase, which makes it a strong candidate material for harsh dry machining condition. On the other hand, it is empirically known that the hardness, toughness and tribological property dominate the wear-resistance of hard coatings, which are dependent upon the coating structure [4]. As a convenient and versatile method, nanocomposite coatings consisting of nanocrystalline/amorphous phase mixture benefit the combination of higher hardness, better toughness, and superior wear-resistance [14,15]. According to the amorphous matrix feature, three groups of nanocomposite hard coatings were clarified: 1. nc-MeN/a-nitride (e.g. a-BN, a-Si_3N_4, etc); 2. nc-MeN(C)/metal (e.g. Cu, Ni, Ag, Y, etc.); 3. nc-MeN(C)/a-C [1]. For instance, Pei, et al. [16,17] deposited TiC/a-C:H nanocomposite coating by magnetron sputtering, and observed that the good toughness together with ultra-low friction coefficient was achieved by modifying acetylene gas rate and substrate bias. However, similar optimized mechanical properties were not commonly observed for all nanocomposite coatings. Yalamanchili et al. [18,19] found that the Zr-Si-N coatings with columnar nanostructure displayed the maximum hardness of 37 GPa, lowest wear

* Corresponding author.
** Corresponding author.
E-mail addresses: kepl@nimte.ac.cn (P. Ke), aywang@nimte.ac.cn (A. Wang).

https://doi.org/10.1016/j.jallcom.2018.11.207
0925-8388/

rate and good fracture toughness. When the nanocomposite structure emerged in the Zr-Si-N coating with increase of Si addition, however, the mechanical and wear-resistance dramatically decreased. The fundamental dependence of nanostructure on the mechanical and tribological performance for hard coatings was still lack of understanding.

Due to the versatile atomic bonds and facile deposition methods, amorphous carbon based coatings provide a great potential for producing hard coatings with tailored nanostructure from nanocolumnar to nanocomposite. By controlling carbon content in coating, EI Mel et al. [20] constructed the Ni/C nanocomposite coatings with different size, distribution, density, and shape of Ni-rich nanoparticulates embedded in a-C matrix. In addition, the combined improvement of mechanical and tribological properties could be achieved when the amorphous carbon (a-C) located in nanocrystalline grain boundaries [21,22]. Yet, various Ti-/Cr-based nanocomposite coatings containing a-C have been fabricated in recent years, such as Ti-C-N, Ti-Al-C-N, Ti-Si-C-N, Cr-Si-C-N, Cr-C-N, etc [23–26], but V-based nanocomposite hard coating has merely been studied. In our previous work, hard and tough V-Al-C-N coatings, where V-based nanocrystalline hard phase was surrounded by sp^2-riched a-C soft phase, were successfully manipulated by a DC sputtering technique [27]. The maximum hardness, H/E ratio, and elastic recovery of V-Al-C-N coatings were ~30 GPa, 0.11 and 69%, respectively, due to the formed special structure. In order to elucidate the carbon effect on nanostructure evolution of the coatings, here we fabricated ternary V-Al-C coatings without introducing nitrogen component, and obtained the microstructure evolution from columnar, nanocolumnar to nanocomposite by changing Ar/CH_4 gas ratio. The relevance between the mechanical and tribological properties of deposited coatings was discussed in terms of microstructural changes. This study not only provides practical guidelines for the design of V-Al-C coating with enhanced combination of wear-resistance and fracture toughness, but also evaluates the possibility of utilizing grain boundary engineering to obtain coatings with excellent working performance.

2. Experimental methods

2.1. Coating preparation

V-Al-C coatings were prepared on the polished high speed steel (HSS) with the size of 15 mm × 15 mm × 3 mm and silicon-(100) substrates using the magnetron sputtering system. The substrates were cleaned ultrasonically in ethanol and acetone for 30 min, respectively, before putting them into the deposition chamber, then the base vacuum was pumped to less 2×10^{-3} Pa. To enhance the adhesion strength, substrates were pre-etched by Ar^+ bombardment for 30 min, and then a Ti interlayer (~300 nm) was deposited using magnetron sputtering. More detailed parameters could be found in elsewhere [28]. Then, V-Al-C coatings were prepared in argon/methane (Ar/CH_4) gas mixture with working pressure varying from 0.8 to 0.95 Pa. During the coating deposition process, Ar with the flow rate of 100 sccm was introduced, while CH_4 flow rate was adjusted from 0, 5, 10, 15 to 20 sccm to regulate carbon content in coatings. Pulsed substrate bias and target to substrates distance were fixed constant at −300 V and 160 mm during all deposition process, respectively. Before characterization, the samples of V-Al-C coating were labeled S-0, S-5, S-10, S-15 and S-20 according to the CH_4 flow rate.

2.2. Characterization

The composition and chemical bonding states of the coatings were determined by XPS (Kratos Axis $ULTRA^{DLD}$). The XPS spectra were obtained after removing the surface layer about 100 nm in situ Ar^+ ions sputtering process and were calibrated by C 1s peak at 284.8 eV. Structure investigations were characterized by the grazing incidence X-ray diffraction (GIXRD, Bruker D8 Advance) equipped with a Cu Kα radiation source (1.5° grazing angle). The cross-sectional morphologies were examined by a SEM (Hitachi S4800). Raman spectra (Renishawin Via-reflex) with the 532 nm laser excitation were applied to assess the sub-structures of carbide and carbon atomic bonds. The spectrum from 200 cm^{-1} to 1800 cm^{-1} covers the acoustic and optical vibration bands of TMC and the disordered graphite bands of a-C. Furthermore, the microstructural characterization of the coatings was obtained by a using high-resolution transmission electron microscopy (HRTEM, FEI TF20).

Hardness and elastic modulus were evaluated in a nano-indentation tester (MTS G200) using a Berkovich indenter with the continuous stiffness mode and Oliver-Pharr method [29], and the indentation depth was about 10% of the coating thickness to avoid the substrate effects. Ten repeated measurements were carried out to minimize the measurement error. Fracture toughness was obtained by the cracks under Vicker's indentation at a load of 500 g. The formed cracks were observed by SEM. At least 3 indentations were conducted and fracture toughness was calculated from average results. The fracture toughness, K_{IC}, was established according to the following formula (1):

$$K_{Ic} = \alpha \left(\frac{E}{H}\right)^{1/2} \left(\frac{P}{C^{3/2}}\right) \quad (1)$$

where K_{IC} is the fracture toughness, E is the elastic modulus, H is the hardness, P is the indentation load, c is the average crack length from the center of the indent to the crack tips, and α is an empirical constant which depends on the indenter geometry. For a Berkovich indenter α is ~0.016 [30].

Tribological measurement was performed by a ball-on-disk reciprocating tests against Al_2O_3 balls (Φ6 mm), where the hardness and elastic modulus of Al_2O_3 balls were 18.5 GPa and 380 GPa, respectively, on the tribometer system (CETR, UMT-3). The tests were carried out under the applied normal load of 5 N, velocity of 5 cm/s and frequency of 5 Hz, and the total sliding time was 1800 s. After that, the section profiles of wear track were performed by a surface profilometer tester. The calculated method about wear rates has been referred to in previous studies [31]. The morphologies and chemical composition of the wear tracks were characterized by SEM equipped with EDX, and the Raman spectra.

3. Results and discussion

3.1. Chemical bonding and phase constitution

The dependence of composition and constitution of the prepared coatings on the various CH_4 flow rate are given in Fig. 1a. With increasing the CH_4 flow rate from 0 to 20 sccm, the C content in the V-Al-C coatings monotonically increased from 37.32 at% to 71.4 at%, while both V and Al content in coatings decreased from 48.52 at% to 18.05 at% and 11.8 at.% to 6.85 at.%, respectively. The concentration of oxygen contaminant in all coatings was found to be lower than 6 at%, possibly resulting from low vacuum degree.

To clarify atomic bonds of carbon in coatings, Fig. 1b shows the typical XPS C 1s spectra of the V-Al-C coatings under various CH_4 flow rates. After being fitted, the spectra of all samples consisted of two peaks at 282.9 eV and 284.8 eV, which could be assigned to C-V and sp^2 C-C bonds respectively. With increasing the CH_4 flow rate from 0 to 20 sccm, the intensity and fraction of C-V bonds

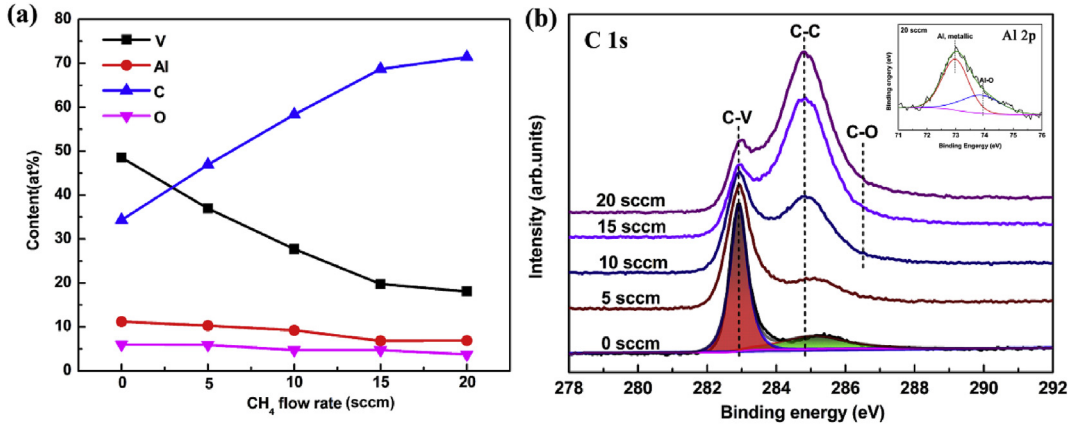

Fig. 1. Chemical composition (a) and C1s XPS spectra (b) of the deposited V-Al-C coatings with various CH_4 flow rates.

decreased, and in contrast those of C-C bonds increased. For the S-0 and S-5, in which the C content was lower than 46.92 at.%, the C-C peaks were weak, suggesting that the C atoms were mainly boned to V atoms. While, the C-C bonds became dominate peak in spectra for S-10 and S-20, where the C content was over 58.33 at.%. Meanwhile, a small amount of C-O bonds appeared in these spectra due to the probable residual oxygen content in gas precursor. Al 2p spectra of the coating S-20 as the representation was shown in the insert of Fig. 1b, suggesting that Al mainly existed in the forms of Al metallic state in addition to some Al-O bonds. Additionally, no peaks of C-Al bonds were identified in all coatings, implying Al might exist in the coatings as solid solution.

Fig. 2 shows the GIXRD results of V-Al-C coating with various CH_4 flow rates. Three diffraction peaks 2θ of about 37.45°, 43.67°and 62.54° could be observed in all coatings, which corresponded to the reflections of VC (111), (200) and (211) phase, respectively. However, three diffraction peaks all shifted towards the higher diffraction angle compared to those of the standard fcc-VC phase (PDF#65-8825), indicating the lattice parameter for the formed VC crystalline in coatings was smaller than that of the ideal fcc-VC phase. The shrunk lattice was probably attributed to the partial substitution of V atoms by smaller Al atoms [32]. According to the combined XRD and XPS results, it could thus be proposed that all V-Al-C coatings showed a NaCl-type fcc-(V, Al)C crystalline structure. Meanwhile, the diffraction peaks from S-5 to S-20 became broader and the intensity of the peaks decreased gradually compared with those of the sample S-0, revealing that the incorporated carbon not only refined the nanocrystallites but also decreased the crystalline degree.

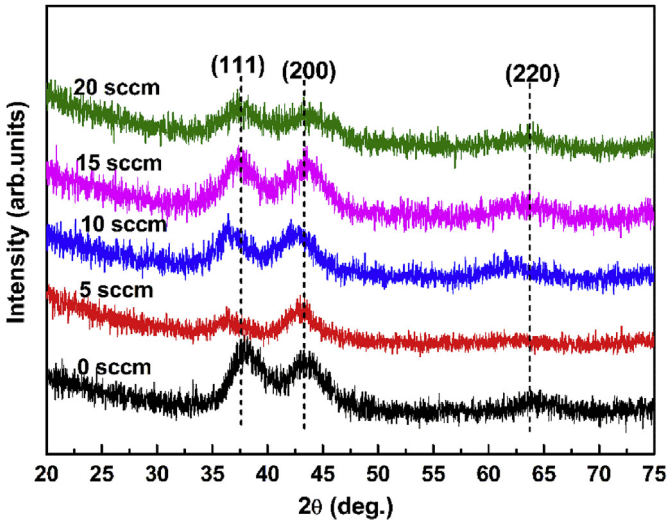

Fig. 2. GIXRD patterns of V-Al-C coating prepared at various CH_4 flow rate.

The hybridized bond structure of the deposited coatings was also assessed by Raman spectroscopy, as shown in Fig. 3. Noted that the presence of two regions was observed, one from 100 to 1000 cm^{-1} resulting from VC compound; another from 1000 to 1800 cm^{-1} originated from the a-C phases [33]. In particular, when the C content was over 58.33 at.%, the appearance of a broad band between 1350 and 1600 cm^{-1} for C-C bonding could be identified to the typical amorphous carbon feature. In general, it can be fitted into two peaks at 1350 cm^{-1} and 1580 cm^{-1}, corresponding to D peak and G peak (shown in Fig. 3b) for the a-C respectively, where the D peak is produced by the breathing mode of only aromatic sp^2 bonds and the G peak originates from sp^2 bonds in both aromatic rings and chains. Since the intensity ratio of D peak to G peak ($I_D/I_G = 2.37$, inserted in Fig. 3b) is closely related to the sp^2 cluster size in C-based coatings, introducing C to V-Al-C coating not only facilitated the formation of a-C, but also preferred to bond as sp^2-C formation in the carbon matrix. Therefore, we could conclude that the coatings for S-0 and S-5 were mainly consisted of (V, Al)C polycrystalline, but the coatings of S-10, S-15 and S-20 were characterized to be nanocomposite structure comprised of (V, Al)C nanocrystallites and sp^2-rich a-C matrix.

3.2. Morphology and nanostructures

The cross-sectional morphologies of V-Al-C coatings with various CH_4 flow rates were shown in Fig. 4. It was clearly seen that the coatings comprised of two layers: one was Ti interlayer of 230 ± 20 nm thickness with obvious columnar structure, and another was 1800 ± 100 nm top-layer V-Al-C coatings. With increasing the C content, the grain refinement of the coatings appeared clearly. For the case of S-0, the coating displayed a wider columnar-type structure, as shown in Fig. 4a. When the CH_4 at 5 sccm was introduced, the morphology of the coating S-5 became fibrous and dense columnar structure (Fig. 4b). Combined with the above-mentioned phase structure analysis, we speculated that the formation of sp^2-rich a-C probably embedded in the grain boundaries, and therefore hindered the grain growth along the lateral direction. Further increasing CH_4 flow rate to 10 sccm, the distinct columnar structure disappeared in the coating accompanying a featureless structure for S-10. This featureless gradually became more compact structure with a smooth surface for case of S-15 and

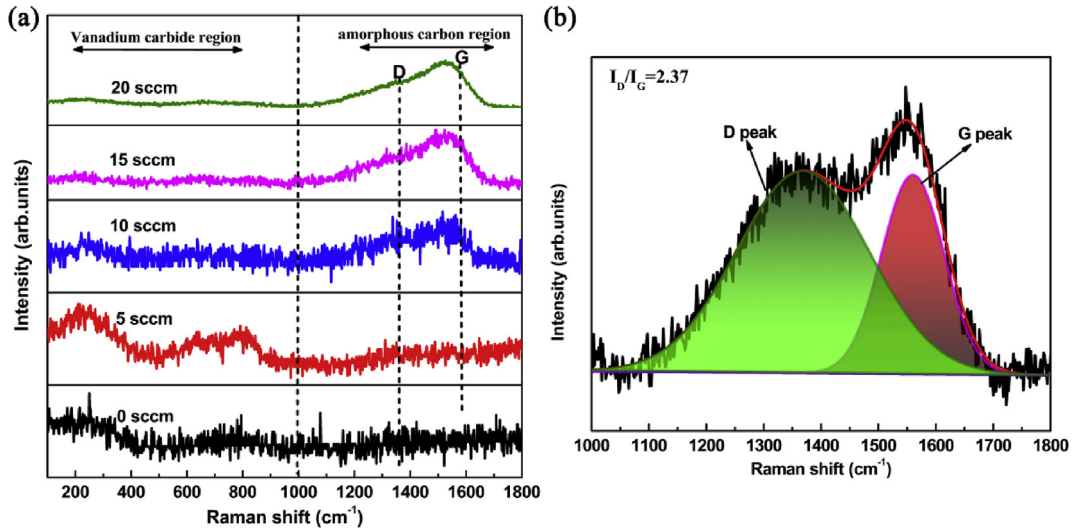

Fig. 3. (a) Raman spectra of the prepared V-Al-C coatings with different CH_4 flow rates (b) Representative Gaussian fitting of Raman peaks of S-10.

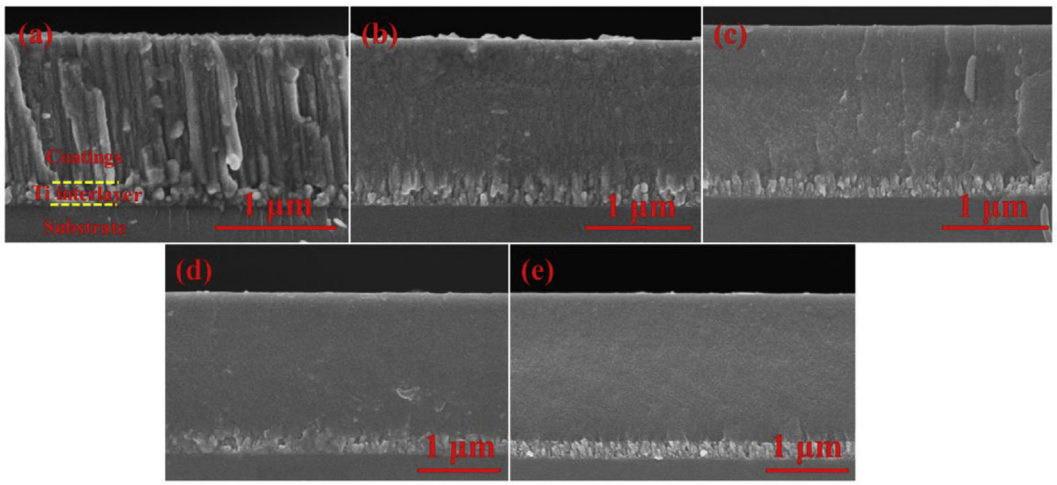

Fig. 4. Cross-section morphologies of the prepared V-Al-C coating with various CH_4 flow rates (a) S-0; (b) S-5; (c) S-10; (d) S-15; (e) S-20.

S-20 coatings. More information about the width of columnar grain and grain size would be discussed in terms of TEM and HRTEM results due to the limited resolution of SEM.

Fig. 5 shows the cross-sectional TEM overview morphologies and corresponding selected area electron diffraction (SAED) of the V-Al-C coatings with various CH_4 flow rates. For the case of S-0, it could be seen from Fig. 5a-b that the coating presented a typical columnar structure with the columnar width of 30–50 nm, elongating the whole coating thickness. The inserted corresponding SAED pattern Fig. 5a was identified to four distinct rings, which assigned to (111), (200), (220) and (311) orientations of fcc-(V, Al)C phase. Noted that the current (311) orientation was not visible in the GIXRD results, this should be attributed to the weak crystalline of the coating or the limited resolution of GIXRD. When the CH_4 was doped (S-5), the columnar nanostructure like nano-pillar was still presented in Fig. 5c-d, but with much finer and shorter columnar width (10–20 nm) compared to that of S-0 case, which was consistent with the SEM results. Further increasing CH_4 flow rate to 10 sccm (S-10), the columnar structure in the coating disappeared, as shown in Fig. 5e-f. Instead, nanoparticles with grain size of 4–8 nm dispersing in the amorphous carbon matrix were shown in Fig. 5e. Moreover, the SAED in the insets exhibited the continuous ring, resulting from the finer nanostructures and the increased carbon content. Further increasing CH_4 flow rate to 15 sccm (S-15, Fig. 5g-h), the coating displayed a nanocomposite structure, which consisted of spherical nanocrystalline (V, Al)C grains distributed in a-C matrix, accompanying with a further reduction of columnar size (3–5 nm), as shown in Fig. 5h. Compared to S-10, however, the SAED patterns inserted in Fig. 5g exhibited the wider and dimmer continuous rings, corresponding to the increased amount of amorphous carbon [34]. In summary, it was made clear that, by controlling the carbon content from 37.32 at.% to 71.4 at.% in V-Al-C coatings, the coating microstructure was tuned accurately from coarse columnar grain to fibrous columnar grains, and finally to nanocomposite structure consisted of the (V, Al)C nanocrystallites and sp^2-rich a-C matrix. Meanwhile, the size, distribution, and shape of (V, Al)C nanocrystallites within a-C matrix could also be controlled well.

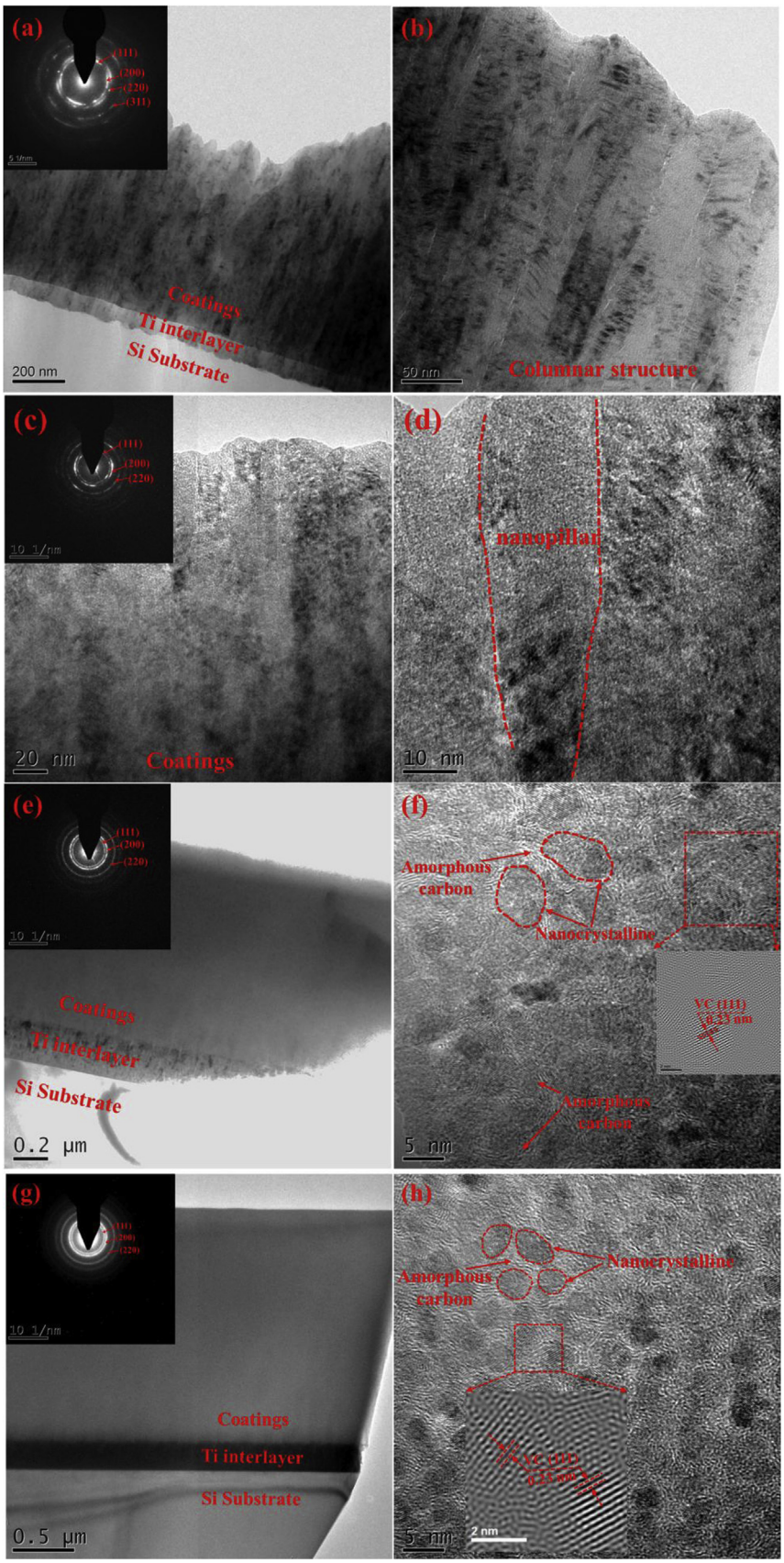

Fig. 5. Cross-sectional TEM image and enlarged view of the S-0 coating (a)(b), S-5 coating (c)(d), S-10 coating (e)(f) and S-15 coating (g)(h).

3.3. Hardness, fracture and tribological properties

The hardness (H) and elastic modulus (E) of the V-Al-C coatings depending on CH_4 flow rate are illustrated in Fig. 6a. It was found that a low H and E value of 14.43 ± 1.7 GPa and 210 ± 5.5 GPa were obtained for S-0, respectively. When 5 sccm CH_4 was introduced, the H and E increased dramatically to 28.74 ± 1.59 GPa and 274 ± 7.2 GPa (S-5), which decreased with further increasing CH_4 from 5 to 15 sccm. But the arresting result was that the reduction degree of hardness was more serious than that of Young's modulus. According to J. Musil's reports [35], the maximum hardness (H_{max}) was achieved at a critical grain size ($d_c \approx 10$ nm). When $d > d_c$, the hardness increased with decreasing grain size based on the Hall-Petch law. While in term of $d < d_c$, the chemical and electronic bonding state between atoms in nanostructure plays a key role. As shown in Fig. 5h, the grain size of coating became smaller than d_c when the CH_4 flow rate increased to 10 sccm, which suggested the finer grain size and the more fraction of a-C, the less hardness and Young's modulus were observed. This result agreed well with the obtained same structure and mechanical properties of binary metal co-doped a-C films [36], especially one carbide-forming metal element and another non-carbide-forming metal one. Li et al. [36] manipulated the Ti/Al co-doped amorphous carbon coatings with various metal content, and found that the hardness ranged from 13.1 ± 0.3 GPa to 16.4 ± 0.3 GPa when the co-doped Ti/Al content changed from $Ti_{1.3\ at.\%}/Al_{2.6\ at.\%}$ to $Ti_{8.5\ at.\%}/Al_{14.4\ at.\%}$.

Fig. 6b shows the H/E and H^3/E^2 ratio of the coatings, representing the resistance against elastic strain to failure and the resistance to plastic deformation, respectively [37,38]. Similar to the tendency of H and E as a function of CH_4 flow rate, the maximum H/E (0.105) and H^3/E^2 (0.318 GPa) value were observed for S-5 coating with CH_4 flow rate of 5 sccm. Since the high H/E ratio can delay elastic to failure and high H^3/E^2 indicates a good resistance to cracks deformation together with cracks propagation, the S-5 coating displayed the best wear-resistance in present situation. Namely, the V-Al-C coating with fibrous columnar structure elongated grains in amorphous matrix benefited the combined excellent fracture toughness and high hardness than those of the coating with nanocomposite structure.

The fracture toughness, K_{IC}, is the ability to resist crack propagation during deformation up to fracture, which is one of the important mechanical properties of a material [39]. Indentation is an empirically used technology to evaluate the fracture property of the coating [40], but the accurate determination of toughness is an open challenge yet. By using a Vickers indentation technique with a load of 5 N, we elucidated the fracture property of the V-Al-C coatings behaving different nanostructure, as shown in Fig. 7. The inserted images in Fig. 7 illustrate the formed in the indentation corners and expanded outwards. The crack length c decreased when the CH_4 was introduced. The calculated fracture toughness of the V-Al-C coatings increased to the maximum of 2.25 MPa $m^{1/2}$ at S-5, where exhibited a nanocolumnar structure, and then gradually declined to 1.1 MPa $m^{1/2}$ at S-20 with nanocomposite structure. These were in accordance with the previous H/E ratio as shown in Fig. 6b. Generally, the fracture toughness of hard coatings was improved via alloying soft phase to form nanocomposite structure or developing metal/ceramic nano-scaled multilayer coatings, suppressing the high stress centered in the ceramic layers [41]. According to our results, the fracture resistance of hard coating was significantly improved by increasing the columnar grain boundaries with lower shear strength, providing the pathway for the crack deflection. This phenomenon of modifying the fracture resistance induced by microstructural was also explored in Zr-Si-N coatings [42].

Fig. 8 shows the tribological properties of V-Al-C coatings with various CH_4 flow rates. The friction coefficient fluctuated severely from 0.5 to 0.7 during the sliding for coating S-0, and the poor wear rates of 3.64×10^{-14} m^3/Nm was achieved. Fig. 9a presents the wear

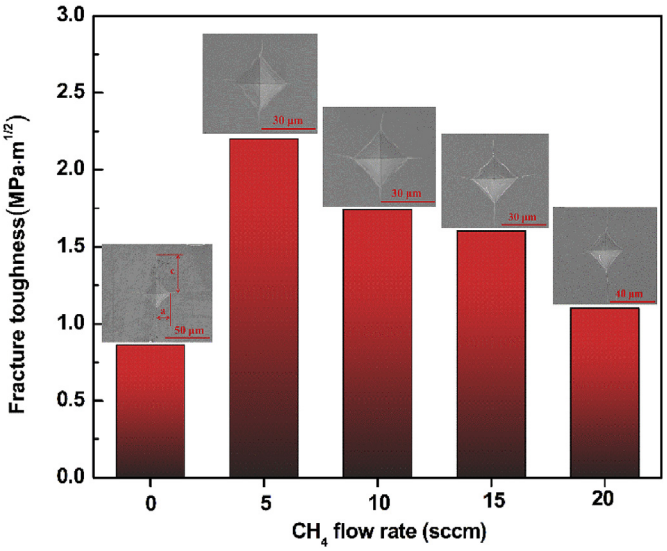

Fig. 7. Fracture toughness and indentation images of the coating prepared under various CH_4 flow rate.

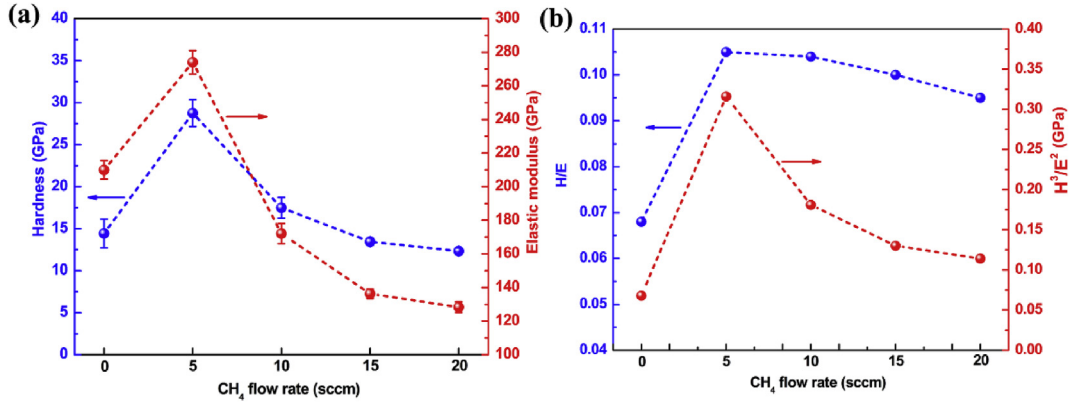

Fig. 6. (a) H, E and (b) H/E, H^3/E^2 value of the V-Al-C coating prepared under various CH_4 flow rates.

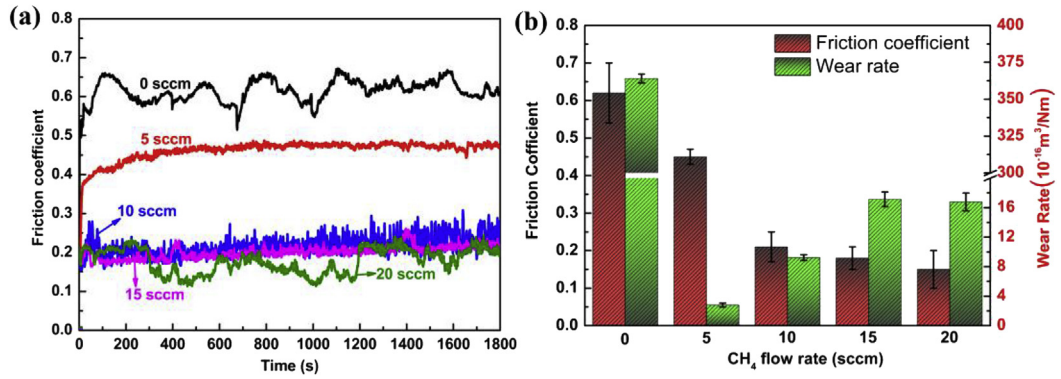

Fig. 8. (a) Friction curve and (b) friction coefficient and wear rates of the V-Al-C coatings prepared under various CH_4 flow rates.

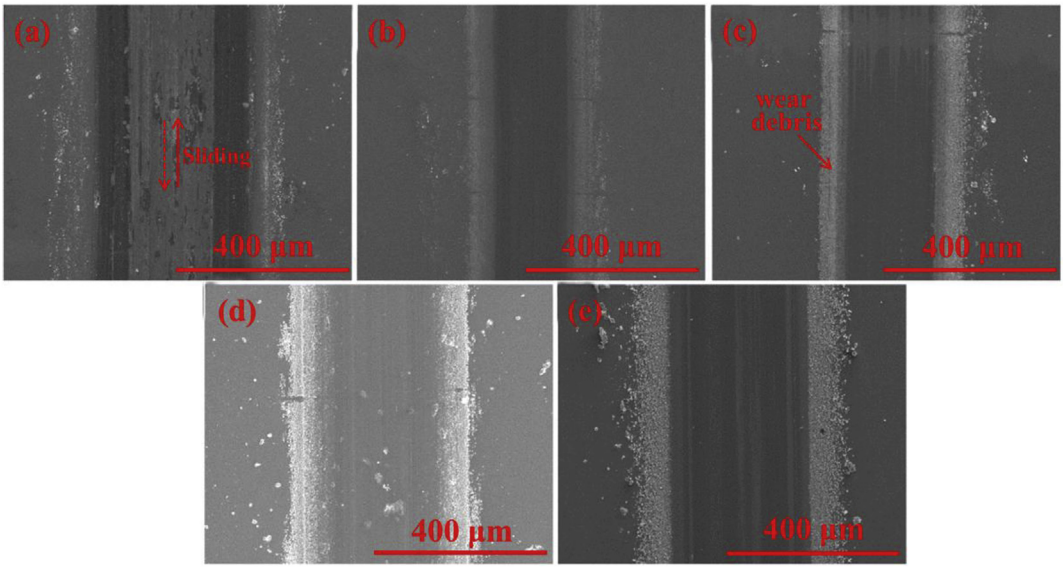

Fig. 9. SEM micrographs of wear tracks of V-Al-C coating prepared under various CH_4 flow rate (a) S-0; (b) S-5; (c) S-10; (d) S-15; (e) S-20.

track morphology, where the wear track was much wider and the coating was worn out. When CH_4 was introduced, the friction coefficient gradually increased to the stable sliding period after a short running-in process. Furthermore, the friction coefficient and wear rates drop to 0.45 and 2.7×10^{-16} m^3/Nm for the coating S-5. When further increasing the CH_4 flow rate, the friction coefficient dramatically decreased to 0.21, and then kept almost constant till S-15. This phenomenon could be attributed to the self-lubrication arising from the formed graphite-like transfer layer induced by the increase of amorphous carbon. However, the friction curves displayed an unusual fluctuation within 0.1–0.2 in case of S-20. From Fig. 9 b-e, the wear tracks for coating S-5 to S-20 seemed to be extremely smooth and no cracks or spalling were found, even the width of wear track showed slight difference. The loose wear debris was evenly distributed on the sides of wear track without severe debris agglomeration. It should be noted that the coating S-5 behaved the lowest wear rate in spite of its relatively high friction coefficient owning to the aforementioned toughness analysis, and the toughness was supposed to be the dominated reason for such excellent wear-resistance, because the coatings with good fracture toughness was usually followed by excellent wear-resistant properties [39].

To clarify the tribological mechanisms, EDS and Raman analysis were carried out for the wear track and wear debris adhered on worn surface of the coating S-15, representatively. As shown in Fig. 10, the obvious oxidation reaction occurred during the sliding, as evidenced from Raman spectrum, where the peaks of V_2O_5 were visible from wear debris [43]. This revealed that the V-based coatings were oxidized and thereafter formed the vanadium oxides during sliding. Since the V_2O_5 Magnéli phase benefits the slipping easier due to lower shear strength [44], the vanadium oxides in deed acted as the lubricants during tribo-process, beyond of the lubricant contribution from graphite like carbon transfer layer induced by amorphous carbon phases. Finally, we could conclude that, after introducing CH_4, the relatively lower friction and lower wear of coating were attributed to the coupling lubrication resulting from the a-C and formed V_2O_5, as well as superior fractural toughness to tolerant deformation.

3.4. Growth mechanism induced by columnar boundaries

To investigate the structural engineering effect on the mechanical and tribological properties of V-Al-C coatings, we can dependently compare the structural evolution with various introduced carbon content. Fig. 11 demonstrated the supposed structural zone diagram with four regions according to the progressive

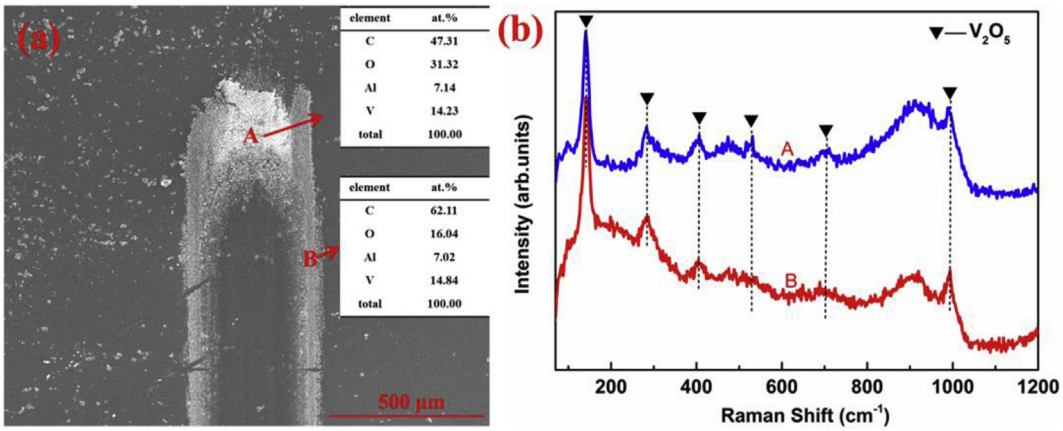

Fig. 10. EDS and Raman analysis wear track of S-15.

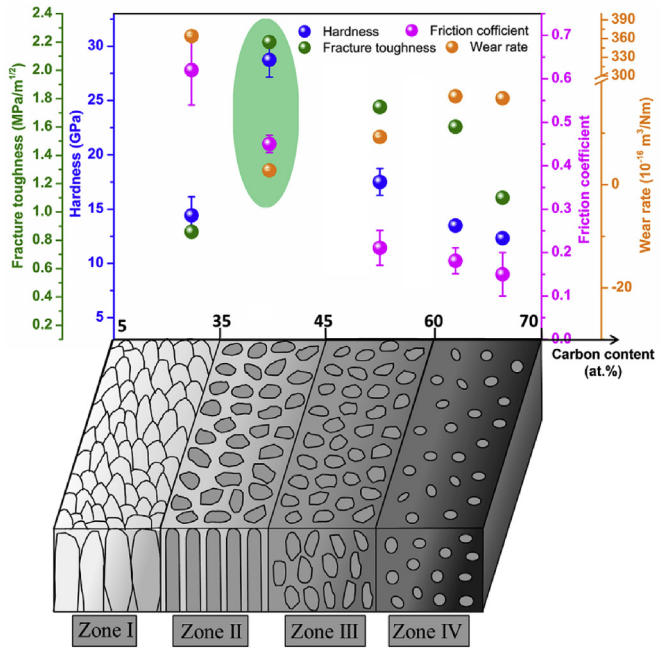

Fig. 11. Structural zone diagram, mechanical and tribological properties as a function of carbon concentration.

structural changes. The zone I represents the typical columnar structure formed in V-Al-C coating, which is governed by the limited atomic mobility on the growth front at low pressure and low temperature during magnetron sputtering technique [45]. Increasing carbon content led to the refining of grain size, corresponding to Zone II, in which the fibrous columnar structure was observed. This could be explicated by the combined effects, including the carbon solubility in metal carbide, the deposited atomic ratio between vanadium and carbon, and atoms diffusion rate. Because of the limited C solubility in metal carbide, the formation of V-Al-C crystallites ejected extra carbon atoms towards the growth front surface with further increase of carbon content [32]. Moreover, the fraction of formed V-Al-C crystallites was quite higher than that of the extra free carbon in Zone II. The extra carbon was dynamically movable under ion bombarding as far as they randomly condensed between the V-Al-C columnar crystals, where columnar boundaries had the lowest total free energy. As a consequence, the condensation of free carbon at the columnar boundaries would block the lateral growth (e.g., parallel to the surface of the substrate) of these V-Al-C columnar crystals, and thereafter, their growth would preferentially elongate the growth direction (e.g., direction perpendicular to the surface of the substrate). Note that no multiphase structure consisting amorphous carbon was identified in such Zone II.

Further increasing the carbon content over 45 at.% led to the reduction of vanadium content in coating, where the extra carbon was involved in the formation of amorphous carbon. Moreover, the existence of Al in the V-Al-C system would contribute to the precipitation of a-C [46]. In this condition, the increased fraction of the accumulated amorphous carbon would significantly suppress the continuous growth of columnar crystallite, as a result of the enhanced coverage rate of carbon and reduced diffusion rate of vanadium. This produced the emergence of a nanocomposite structure with discrete spherical or elongated nano-particles surrounded by a-C matrix (shown in Zone III and IV). Thus, it could be clarified that the modulation of the V-Al-C crystallites was originated from a competition between phase separation and continuous deposition of sputtered particles on the surface [45]. If the growth rate of V-Al-C crystallites along the deposition direction was kinetically slight faster than the deposition rate of carbon, the elongated V-Al-C nanocrystallites would be the dominated structures, as illustrated as Zone III in Fig. 11. However, once the vertical growth of V-Al-C crystallite was quite lower than the coverage rate of carbon, the shape of the V-Al-C nanocrystallites changed to the spherical structure surrounded by amorphous carbon, as shown in Zone IV [20].

Regarding the combined evolution of structure and physical properties of V-Al-C coating in Zone II, it was clear that the fibrous columnar structure benefited both the highest hardness of 28.74 GPa and fracture toughness of 2.25 MPa $m^{1/2}$, which thereafter rendered the lowest wear rate of 2.7×10^{-16} m^3/Nm. In general, when the adhesive energy of the interface is much lower than the cohesive energy of the coating, the crack will be diverted to the interface. The literature on indentation-induced fracture studies have indicated, for multilayer coatings, that the incoherent interfaces between the layers offered the pathway for crack deflection and additional energy dissipation [47–49]. While in case of the monolithic coatings, the crack deflection occurred on the columnar grain boundaries regions with lower shear strength. In our case, increasing the carbon content in V-Al-C monolithic coatings to an optimized range (Zone II), the refined columnar grain and improved interface density were obtained. Therefore, the

formation of larger columnar boundaries was inhibited, and the microcrack initiation or propagation in coating was suppressed significantly under load, as evidenced by the improved fracture toughness. In addition, if one connected the correlation between grain size evolution and hardness changes in terms of Hall-Petch relation, the enhanced hardness shown in Zone II could be easily understood by the reduced grain size of (V, Al)C nano-crystallites. Further increasing the carbon content led to the increased sp^2-rich amorphous carbon, as demonstrated in Zone III and Zone IV, which played the key role in the reduction of hardness and toughness of these V-Al-C coatings [50].

4. Conclusion

The microstructures, mechanical and tribological properties of V-Al-C coatings as a function of carbon content were systematically studied in this work. The results indicated that, as the carbon content varying from 37.32 at.% to 71.4 at.%, significant structure changes were tuned from coarse columnar grains to fibrous columnar grains and finally to nanocomposite structure, consisting of the (V,Al)C nanocrystallites and sp^2-rich a-C phases. Additionally, the size, distribution, and the shape of (V,Al)C nano-crystallites could be well controlled. The V-Al-C coating (S-5) with carbon content of 37.32 at.% exhibited the fibrous columnar structure, when the maximum hardness of 28.74 GPa and good toughness of $H/E > 0.1$ were obtained, respectively. With further increasing the carbon content, nanocomposite structure began to emerge in the coating, accompanied by reducing the hardness and friction coefficient, which could be attributed to the increased content of a-C and the coupling lubrication of both a-C and V_2O_5 Magnéli phase. The important result in this study was that the V-Al-C coating with tailored fibrous columnar microstructure yielded the combined high hardness, good fracture toughness and the superior wear-resistance. This brings forward a promising and facile strategy to fabricate the hard yet tough wear-resistant coating via grain boundary engineering.

Acknowledgments

The research was supported by the National Natural Science Foundation of China (51522106, 51875555, 51611130061), Project of Jiangxi Province (2018-YZD2-15) and Zhejiang Provincial Natural Science Foundation (LQ19E010002). We all sincerely thank Xin Wang for useful help in experiments and discussion.

References

[1] J. Musil, Hard and superhard nanocomposite coatings, Surf. Coating. Technol. 125 (2000) 322–330.
[2] J.M.F. de Paiva, R.D. Torres, F.L. Amorim, D. Covelli, M. Tauhiduzzaman, S. Veldhuis, G. Dosbaeva, G. Fox-Rabinovich, Frictional and wear performance of hard coatings during machining of superduplex stainless steel, Int. J. Adv. Manuf. Technol. 92 (2017) 423–432.
[3] R. Haubner, M. Lessiak, R. Pitonak, A. Köpf, R. Weissenbacher, Evolution of conventional hard coatings for its use on cutting tools, Int. J. Refract. Met. Hard 62 (2017) 210–218.
[4] P.H. Mayrhofer, C. Mitterer, L. Hultman, H. Clemens, Microstructural design of hard coatings, Prog. Mater. Sci. 51 (2006) 1032–1114.
[5] D. Music, R.W. Geyer, J.M. Schneider, Recent progress and new directions in density functional theory based design of hard coatings, Surf. Coating. Technol. 286 (2016) 178–190.
[6] B. Syed, J. Zhu, P. Polcik, S. Kolozsvari, G. Håkansson, L. Johnson, M. Ahlgren, M. Jöesaar, M. Odén, Morphology and microstructure evolution of Ti-50 at.% Al cathodes during cathodic arc deposition of Ti-Al-N coatings, J. Appl. Phys. 121 (2017), 245309.
[7] A. Miletić, P. Panjan, B. Škorić, M. Čekada, G. Dražič, J. Kovač, Microstructure and mechanical properties of nanostructured Ti–Al–Si–N coatings deposited by magnetron sputtering, Surf. Coating. Technol. 241 (2014) 105–111.
[8] M. Azzi, M. Benkahoul, J.A. Szpunar, J.E. Klemberg-Sapieha, L. Martinu, Tribological properties of CrSiN-coated 301 stainless steel under wet and dry conditions, Wear 267 (2009) 882–889.
[9] Q. Ma, F. Zhou, S. Gao, Z. Wu, Q. Wang, K. Chen, Z. Zhou, L.K.-Y. Li, Influence of boron content on the microstructure and tribological properties of Cr-B-N coatings in water lubrication, Appl. Surf. Sci. 377 (2016) 394–405.
[10] V. Moraes, H. Bolvardi, S. Kolozsvári, H. Riedl, P.H. Mayrhofer, Thermal stability and mechanical properties of Ti-Al-B-N thin films, Int. J. Refract. Met. Hard 71 (2018) 320–324.
[11] Z.H. Cai, H. Qin, X.K. Du, Z. Yang, Compositional, structural and mechanical properties of (Ti,Cr,Al)N coatings deposited on the surface of piston rings, Appl. Mech. Mater. 584–586 (2014) 1495–1499.
[12] N. Fateh, G.A. Fontalvo, G. Gassner, C. Mitterer, The beneficial effect of high-temperature oxidation on the tribological behaviour of V and VN coatings, Tribol. Lett. 28 (2007) 1–7.
[13] N. Fateh, G.A. Fontalvo, G. Gassner, C. Mitterer, Influence of high-temperature oxide formation on the tribological behaviour of TiN and VN coatings, Wear 262 (2007) 1152–1158.
[14] J. Musil, Flexible hard nanocomposite coatings, RSC Adv. 5 (2015) 60482–60495.
[15] K.M. Jiang, D.Q. Zhao, X. Jiang, Q. Huang, L.J. Miao, H.M. Lu, Y. Li, Electronic-structure, corrosion and mechanical properties of nc-CrC/a-C:H films deposited by multi-arc ion plating, J. Alloys Compd. 750 (2018) 560–569.
[16] Y.T. Pei, D. Galvan, J.T.M. De Hosson, C. Strondl, Advanced TiC/a-C:H nanocomposite coatings deposited by magnetron sputtering, J. Eur. Ceram. Soc. 26 (2006) 565–570.
[17] Y. Pei, D. Galvan, J. Dehosson, Nanostructure and properties of TiC/a-C:H composite coatings, Acta Mater. 53 (2005) 4505–4521.
[18] K. Yalamanchili, R. Forsen, E. Jimenez-Pique, M.P.J. Joesaar, J.J. Roa, N. Ghafoor, M. Oden, Structure, deformation and fracture of arc evaporated Zr-Si-N hard films, Surf. Coating. Technol. 258 (2014) 1100–1107.
[19] K. Yalamanchili, E. Jimenez-Pique, L. Pelcastre, K.D. Bakoglidis, J.J. Roa, M.P.J. Joesaar, B. Prakash, N. Ghafoor, M. Oden, Influence of microstructure and mechanical properties on the tribological behavior of reactive arc deposited Zr-Si-N coatings at room and high temperature, Surf. Coating. Technol. 304 (2016) 393–400.
[20] A.A. El Mel, E. Grigore, E. Gautron, A. Granier, B. Angleraud, P.Y. Tessier, Shape control of nickel nanostructures incorporated in amorphous carbon films: from globular nanoparticles toward aligned nanowires, J. Appl. Phys. 111 (2012), 114309.
[21] D.M.-M.J.C. Sánchez-López, C. López-Cartes, A. Fernández, Tribological behaviour of titanium carbide/amorphous carbon nanocomposite coatings: from macro to the micro-scale, Surf. Coating. Technol. 202 (2008) 4011–4018.
[22] M. Stueber, P.B. Bama, M.C. Simmonds, U. Albers, H. Leiste, C. Ziebert, H. Holleck, A. Kovacs, P. Hovsepian, I. Gee, Constitution and microstructure of magnetron sputtered nanocomposite coatings in the system Ti-Al-N-C, Thin Solid Films 493 (2005) 104–112.
[23] J. Hu, X. Tian, M. Yang, C. Gong, J. Lin, Improvement of discharge and microstructure of Cr-C-N coatings by electromagnetically enhanced magnetron sputtering, Vacuum 148 (2018) 98–105.
[24] J. Li, Y. Wang, Y. Yao, Y. Wang, L. Wang, Structure and tribological properties of TiSiCN coating on Ti6Al4V by arc ion plating, Thin Solid Films 644 (2017) 115–119.
[25] Z. Wu, F. Zhou, Q. Wang, Z. Zhou, L.K.-Y. Li, Comparisons of tribological and electrochemical properties of CrSiC and CrSiCN coatings in seawater, Surf. Coating. Technol. 340 (2018) 137–144.
[26] E. Thangavel, S. Lee, K.-S. Nam, J.-K. Kim, D.-G. Kim, Synthesis and characterization of Ti–Si–C–N nanocomposite coatings prepared by a filtered vacuum arc method, Appl. Surf. Sci. 265 (2013) 60–65.
[27] Z.Y. Wang, X. Li, X. Wang, S. Cai, P. Ke, A. Wang, Hard yet tough V-Al-C-N nanocomposite coatings: microstructure, mechanical and tribological properties, Surf. Coating. Technol. 304 (2016) 553–559.
[28] C. Kong, P. Guo, L. Sun, Y. Zhou, Y. Liang, X. Li, P. Ke, K.-R. Lee, A. Wang, Tribological mechanism of diamond-like carbon films induced by Ti/Al co-doping, Surf. Coating. Technol. 342 (2018) 167–177.
[29] W. Yan, C.L. Pun, G.P. Simon, Conditions of applying Oliver–Pharr method to the nanoindentation of particles in composites, Compos. Sci. Technol. 72 (2012) 1147–1152.
[30] B. Bhushan, X.D. Li, Nanomechanical characterisation of solid surfaces and thin films, Int. Mater. Rev. 48 (2013) 125–164.
[31] Z.Y. Wang, X.W. Li, J. Zhou, P. Liu, Q. Huang, P.L. Ke, A.Y. Wang, Microstructure evolution of V-Al-C coatings synthesized from a V_2AlC compound target after vacuum annealing treatment, J. Alloys Compd. 661 (2016) 476–482.
[32] Q. Luo, S.C. Wang, Z. Zhou, L. Chen, Structure characterization and tribological study of magnetron sputtered nanocomposite nc-TiAlV(N,C)/a-C coatings, J. Mater. Chem. 21 (2011) 9746.
[33] L. Escobar-Alarcon, V. Medina, E. Camps, S. Romero, M. Fernandez, D. Solis-Casados, Microstructural characterization of Ti-C-N thin films prepared by reactive crossed beam pulsed laser deposition, Appl. Surf. Sci. 257 (2011) 9033–9037.
[34] Q.M. Wang, K.H. Kim, Microstructural control of Cr-Si-N films by a hybrid arc ion plating and magnetron sputtering process, Acta Mater. 57 (2009) 4974–4987.
[35] J. Musil, Hard nanocomposite coatings: thermal stability, oxidation resistance and toughness, Surf. Coating. Technol. 207 (2012) 50–65.
[36] X. Li, P. Guo, L. Sun, X. Zuo, D. Zhang, P. Ke, A. Wang, Ti/Al co-doping induced residual stress reduction and bond structure evolution of amorphous carbon

films: an experimental and ab initio study, Carbon 111 (2017) 467–475.
[37] A. Leyland, A. Matthews, Design criteria for wear-resistant nanostructured and glassy-metal, Surf. Coating. Technol. 177 (2004) 317–324.
[38] Q.Z. Wang, Z.W. Wu, F. Zhou, J.W. Yan, Comparison of crack resistance between ternary CrSiC and quaternary CrSiCN coatings via nanoindentation, Mater. Sci. Eng. A Struct. 642 (2015) 391–397.
[39] Y.T. Pei, P. Huizenga, D. Galvan, J.T.M. De Hosson, Breakdown of the Coulomb friction law in TiC/a-C:H nanocomposite coatings, J. Appl. Phys. 100 (2006), 114309.
[40] R. Chen, J.P. Tu, D.G. Liu, Y.J. Mai, C.D. Gu, Microstructure, mechanical and tribological properties of TiCN nanocomposite films deposited by DC magnetron sputtering, Surf. Coating. Technol. 205 (2011) 5228–5234.
[41] C. Wang, K. Shi, C. Gross, J.M. Pureza, M. de Mesquita Lacerda, Y.-W. Chung, Toughness enhancement of nanostructured hard coatings: design strategies and toughness measurement techniques, Surf. Coating. Technol. 257 (2014) 206–212.
[42] K. Yalamanchili, E. Jiménez-Piqué, L. Pelcastre, K.D. Bakoglidis, J.J. Roa, M.P. Johansson Jöesaar, B. Prakash, N. Ghafoor, M. Odén, Influence of microstructure and mechanical properties on the tribological behavior of reactive arc deposited Zr-Si-N coatings at room and high temperature, Surf. Coating. Technol. 304 (2016) 393–400.
[43] M.V. Bosco, M.A. Banares, M.V. Martinez-Huerta, A.L. Bonivardi, S.E. Collins, In situ FTIR and Raman study on the distribution and reactivity of surface vanadia species in V_2O_5/CeO_2 catalysts, J. Mol. Catal. A Chem. 408 (2015) 75–84.
[44] R. Franz, C. Mitterer, Vanadium containing self-adaptive low-friction hard coatings for high-temperature applications: a review, Surf. Coating. Technol. 228 (2013) 1–13.
[45] G. Abrasonis, G.J. Kovács, L. Ryves, M. Krause, A. Mücklich, F. Munnik, T.W.H. Oates, M.M.M. Bilek, W. Möller, Phase separation in carbon-nickel films during hyperthermal ion deposition, J. Appl. Phys. 105 (2009), 083518.
[46] M. Lindquist, O. Wilhelmsson, U. Jansson, U. Wiklund, Tribofilm formation and tribological properties of TiC and nanocomposite TiAlC coatings, Wear 266 (2009) 379–387.
[47] K. Yalamanchili, F. Wang, H. Aboulfadl, J. Barrirero, L. Rogström, E. Jiménez-Pique, F. Mücklich, F. Tasnadi, M. Odén, N. Ghafoor, Growth and thermal stability of TiN/ZrAlN: effect of internal interfaces, Acta Mater. 121 (2016) 396–406.
[48] C. Dang, J. Li, Y. Wang, J. Chen, Structure, mechanical and tribological properties of self-toughening TiSiN/Ag multilayer coatings on Ti6Al4V prepared by arc ion plating, Appl. Surf. Sci. 386 (2016) 224–233.
[49] X. Sui, J. Liu, S. Zhang, J. Yang, J. Hao, Microstructure, mechanical and tribological characterization of CrN/DLC/Cr-DLC multilayer coating with improved adhesive wear resistance, Appl. Surf. Sci. 439 (2018) 24–32.
[50] T.Z. Jorg Patscheider, Matthieu Diserens, Structure–performance relations in nanocomposite coatings, Surf. Coating. Technol. 146–147 (2001) 201–208.